JOURNAL OF NANO AND MATERIALS SCIENCE RESEARCH
Volume 3, No.2 (Special Issue, 2025), pp. 28 – 35
Available online at journals.nanotechunn.com/jnmsr

ORIGINAL ARTICLE

Enhanced Bandgap Energy of Zirconium Doped Chromium Sulphide Material Synthesized via Electrochemical Deposition Technique

*Laeticia U. Ugwu [a,c], Imosobomeh L. Ikhioya[b] *, Azubuike J. Ekpunobi[c]*

[a]*Department of Physics Education, Federal College of Education (Technical) Umunze, Anambra State, Nigeria*
[b]*Department of Physics, Federal University Lokoja, Kogi State Nigeria.*
[c]*Department of Physics and Industrial Physics, Nnamdi Azikiwe University, Awka, Nigeria*

KEYWORDS

CrS, Zr/CrS, Band gap, Metal, Electrodeposition

ARTICLE HISTORY

Received: February 10, 2025
Revised: June 12, 2025
Accepted: June 26, 2025
Published: August 12, 2025

ABSTRACT

In this study, the electrochemical deposition was used to synthesize Zr-doped CrS for photovoltaic application. The XRD diffraction angle of CrS and Zr-doped CrS material at 2θ = 25.256º and 27.009º confirmed the existence of CrS and Zr-doped CrS material. The diffraction peaks at 2θ = 25.256º, 30.329º, 34.426º, 41.198º, 45.678º, 56.389º and 65.231º correspond respectively to the diffraction planes of 111, 112, 116, 200, 201, 211 and 300 of CrS materials. And the diffraction peaks at 2θ = 27.009º, 34.321º, 38.471º, 52.345º, 55.177º, 62.397º and 66.548º correspond respectively to the diffraction planes of 111, 112, 116, 200, 201, 211 and 300 of Zr-doped CrS materials. The analysis reveals that the films contain nanoparticles of various sizes, from a few nanometers to tens of nanometers. At a dopant concentration of 0.01 M, the nanoparticles aggregate and have irregular shapes. When the concentration reaches 0.03 M, the irregular particles change into nano balls. The energy bandgap of CrS is 2.35 eV, but when Zr is doped into CrS, the energy bandgap ranges from 2.01 to 1.55 eV.

* **CORRESPONDING AUTHOR** | I. L. Ikhioya, ✉ imosobomeh.ikhioya@fulokoja.edu.ng

1 Introduction

The industrial revolution has led to a substantial rise in carbon dioxide (CO_2) emissions into the environment in recent years. The usage of fossil fuels primarily caused this exponential increase in CO_2 emissions. Converting light energy into electricity, photovoltaic systems provide a promising alternative for a carbon-free society. Conventional amorphous and crystalline silicon solar cells currently control around 95% of the photovoltaics market. The reason is their easy accessibility and high-power conversion efficiencies in outdoor lighting. However, conventional Si solar cells have drawbacks, including fragility, fixed bandgaps, low absorption rates, complicated manufacturing methods, and weak performance indoors [1]. Therefore, these limitations restrict their use in self-powered wearables, implants, and architecture applications.

2D transition metal dichalcogenides (TMDs) are bringing great promise to the semiconductor field, particularly in high-specific power technologies for photovoltaics. TMDs possess adjustable energy band structures, high carrier mobilities, and exceptional optical transparency. TMDs have the potential to reach light absorption coefficients that are ten times higher than those of traditional direct-bandgap semiconductors. Self-passivated surfaces and nearly perfect band gaps enable efficient solar energy capture [2]–[7].

TMDs, at a thickness of only 20 nm, can absorb nearly all light in the visible spectrum. Thus, TMDs with band gaps between 1.0 and 2.5 eV work well for both single-junction and tandem double-junction solar cells. The absence of surface dangling bonds in stacked TMDs allows for the creation of lattice-mismatch-free heterostructures. This improves the efficiency of the photovoltaic process. These advantages expand the design possibilities in TMD-based photovoltaics [8]–[13].

Two-dimensional materials allow for the creation of intricate multilayer systems that traditional electrochemical deposition techniques cannot produce due to the principles of electrolysis. Artificially engineered vertical 2D heterostructures exhibit fascinating physical and chemical properties, different from 3D materials. The discovery of unconventional superconductivity in twisted bilayer graphene opens up new possibilities for finding high-temperature superconductors. Recently developed 2D heterostructures that merge organic and inorganic materials have showed enhanced mechanical and energy storage capabilities [14]–[19].

The demand for harnessing solar energy is increasing daily because of insufficient electricity from other sources. The depletion of resources and environmental issues are being exacerbated by the use of petroleum fuels in thermal power plants. Converting and storing renewable energy sources, like solar energy, is essential as nonrenewable fossil fuels dwindle and contribute to environmental issues. Global scientists are searching for earth abundant materials and composites to produce affordable, stable, and clean energy through solar power.

Photovoltaic technology, materials, and devices enable the conversion of sunlight into electricity. Semiconductor p-n junctions enable solar cells to convert sunlight into electricity [20], [21]. Electron-hole pairs are generated in the semiconductor when light of a specific wavelength reaches the p-n junction, and the junction barrier subsequently separated them. The study of metal chalcogenide thin films has received significant attention in recent years due to their potential uses in photovoltaic and opto-electronic devices. Solar photovoltaic power is a highly promising solution for the global energy crisis. For solar cells to be competitive, they must be both reliable and cost effective. Wafer, thin film, and organic solar technologies have undergone extensive research and achieved remarkable success in terms of reliability, cost-effectiveness, and efficiency.

Crystalline silicon has proven highly successful in transitioning from the lab to commercial use, with a dominating 90% share of the global PV market. Using less material and increasing energy conversion efficiency shows cost effectiveness. Wafer technology achieves high efficiency, while thin films minimize material usage. Simultaneously meeting both goals is necessary for low-cost electricity production and widespread adoption of solar power. The three most commonly used thin film solar cells are α-Si, CdTe, and CIGS. All three materials have a direct band gap, allowing for the use of thin layers. Their temperature coefficient is very low. Building integrated photovoltaics can include the incorporation of three technologies. Consumer electronics like calculators and watches primarily utilize the amorphous silicon solar cell.

In this study, we used electrochemical deposition to synthesize Zr-doped CrS for photovoltaic application and we conducted a characterization of the synthesized films for their optical, electrical, structural, and surface morphological analysis.

2 Experimental Procedure

The electrochemical deposition technique was used to synthesize CrS and Zr-doped CrS material. The chromium (III) chloride ($CrCl_3.6H_2O$), zirconium (IV) oxychloride octahydrate ($ZrOCl_2.8H_2O$), Thioacetamide (C_2H_5NS), are part of the electrochemical bath system. A magnetic stirrer was used to stir the reaction bath. The electric field (DC voltage) was generated by the power supply, with the cathode made of conducting glass and the anode composed of carbon and fluorine electrodes. The consistent thin film deposition was achieved through electrochemical deposition.

The FTO-coated working electrode, measuring 2.5 cm × 1.5 cm, was fragmented and cleaned with dishwashing liquid. To deposit CrS and Zr-doped CrS, mix 0.01 mol of chromium (III) chloride ($CrCl_3.6H_2O$), zirconium (IV) oxychloride octahydrate ($ZrOCl_2.8H_2O$), Thioacetamide (C_2H_5NS). Three electrodes are utilized in the synthesis process. Platinum is used for the anode, while the reference electrode consists of silver and silver chloride (Ag/AgCl), and the cathode is made of FTO (fluorine-doped tin oxide). The counter and reference

electrodes were vertically placed in the beaker on the FTO-coated substrate.

To synthesize, maintain a potentiostatic condition of -200 mV versus SCE for 5 seconds. The synthesized films were cleaned and dried using the hand dryer. During synthesis, target materials and precursors were poured into beakers in equal amounts. The films underwent a 20-minute annealing treatment to relieve internal stress. The optical, structural, elemental, and electrical characteristics of the synthesized materials were thoroughly assessed using appropriate tools.

3 Results and Discussions

3.1 *Structural Analysis of CrS and Zr-doped CrS Deposited At Different Molar Concentrations*

The XRD study reveals the crystal structures of CrS and Zr-doped CrS material, as presented in Figure 1. The XRD diffraction angle of CrS and Zr-doped CrS material at 2θ=25.256° and 27.009° confirmed the characteristic peak of CrS and Zr-doped CrS material. The diffraction peaks at 2θ = 25.256°, 30.329°, 34.426°, 41.198°, 45.678°, 56.389° and 65.231° correspond respectively to the diffraction planes of 111, 112, 116, 200, 201, 211 and 300 of CrS materials. And the diffraction peaks at 2θ=27.009°, 34.321°, 38.471°, 52.345°, 55.177°, 62.397° and 66.548° correspond respectively to the diffraction planes of 111, 112, 116, 200, 201, 211 and 300 of Zr-doped CrS materials.

Equation 1 was used to calculate the size of the material's crystallite. The analysis in Table 1 is the calculated crystallite size of CrS and Zr-doped CrS materials. Changing the concentration from 0.01 to 0.03 M leads to structural modifications in both CrS and Zr-doped CrS materials during deposition. This process influences the material's properties and performance. The CrS and Zr-doped CrS material's crystallite size grows as the molarity rises. This suggests an improvement in the crystallinity and growth of the material's grains. Molar concentration can significantly affect the crystal structure of CrS and Zr-doped CrS films. these studies have shown that increasing the molar concentration of the precursor solution can lead to changes in the film's crystallinity, phase composition, and crystallite size.

$$D = \frac{k\lambda}{\beta cos\theta} \quad (1)$$

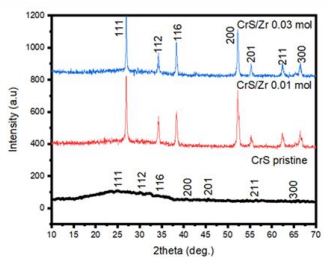

Figure 1: XRD pattern of CrS and Zr-doped CrS

Table 1: CrS and Zr-doped CrS structural properties

Films	2θ (deg.)	d (spacing) Å	(Å)	(β)	(hkl)	(D) nm	σ lines/m^2 X 10^{15}
CrS pristine	25.256	3.525	6.106	0.5902	111	2.390	5.133
	30.329	2.946	5.893	0.5961	112	2.384	5.236
	34.426	2.604	5.209	0.5972	116	2.353	5.148
	41.198	2.190	4.898	0.5974	200	2.418	4.947
	45.678	1.985	4.864	0.5977	201	2.417	4.800
	56.389	1.631	4.614	0.5979	211	2.416	4.393
	65.231	1.430	4.044	0.5981	300	2.415	4.015
CrS/Zr 0.01 mol	27.009	3.300	5.717	0.5531	111	2.550	4.575
	34.321	2.612	5.224	0.5534	112	2.568	4.423
	38.471	2.339	4.679	0.5536	116	2.538	4.322
	52.345	1.747	3.907	0.5538	200	2.609	3.908
	55.177	1.664	4.076	0.5541	201	2.607	3.815
	62.397	1.488	4.208	0.5543	211	2.606	3.556
	66.548	1.404	3.973	0.5546	300	2.605	3.401
CrS/Zr 0.03 mol	27.009	3.300	5.717	0.5356	111	2.634	4.290
	34.321	2.612	5.224	0.5362	112	2.651	4.152
	38.471	2.339	4.679	0.5363	116	2.620	4.056
	52.345	1.747	3.907	0.5371	200	2.690	3.675
	55.177	1.664	4.076	0.5372	201	2.689	3.586
	62.397	1.488	4.208	0.5373	211	2.689	3.341
	66.548	1.404	3.973	0.5382	300	2.684	3.203

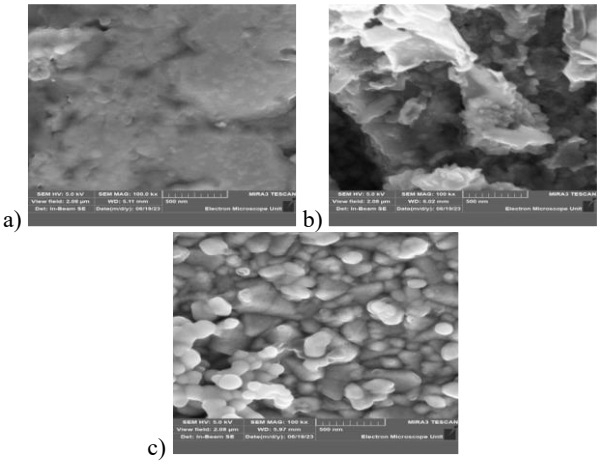

Figure 2: Surface morphology of a.) CrS b.) 0.01 Zr-doped CrS/Zr and c.) 0.03 Zr-doped CrS/Zr films

3.2 *Surface Morphology Analysis of CrS and Zr-doped CrS Material Deposited At Different Molar Concentration*

Figure 2 illustrates the surface morphology of chromium sulphide (CrS) and Zr-doped CrS films deposited at various molar concentrations. The deposition technique and parameters used have a significant impact on the micrograph. The surface reveals that the films contain nanoparticles of various sizes, from a few nanometers to tens of nanometers. At a dopant concentration of 0.01 M, the nanoparticles aggregate and have irregular shapes. When the concentration reaches 0.03 M, the irregular particles change into nano balls. Zirconium dopant enhances the surface morphology of the deposited films, making them suitable for photovoltaic applications.

The micrograph reveals that the surface of CrS films is smooth, compact, and has dispersed grains. The films exhibit a porous and interconnected network structure with nano balls and grains at a concentration of 0.03 M. The formation of CrS and Zr-doped CrS is evident in energy dispersive X-ray (EDX) presented in Figure 3.

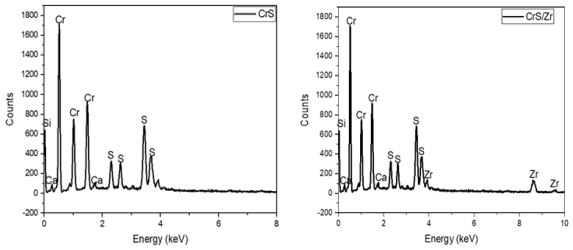

Figure 3: EDXs spectrum of CrS and Zr-doped CrS

The Table 2 represents the variation of electrical properties of the prepared (CrS/Zr) samples with concentration. For the CrS/Zr samples, it is observed that the resistivity fluctuates between 5.29×10^5 Ωm and 3.92×10^5 Ωm as the Zr concentration increases from 0.00 M to 0.03 M. The electrical conductivity fluctuates oppositely as resistivity between 1.89×10^4 Ωm and 2.55×10^4 Ωm as the Zr concentration increases from 0.00 M to 0.03 M. The lowest value of resistivity is obtained when the Zr ions concentration reaches the maximum value of 0.03 M.

Figure 4 depicts the relationship between resistivity and conductivity with deposition parameter.

Table 2: Electrical study of chromium sulphide and chromium sulphide doped zirconium synthesize at different zirconium molarity

Samples	Thickness, t (nm)	Resistivity, ρ (Ω.m)	Conductivity, σ (S/m)
CrS	109.73	5.29×10^5	1.89×10^4
CrS/Zr 0.01 mol	105.43	4.92×10^5	2.03×10^4
CrS/Zr 0.02 mol	104.78	4.84×10^5	2.06×10^4
CrS/Zr 0.03 mol	104.98	3.92×10^5	2.55×10^4

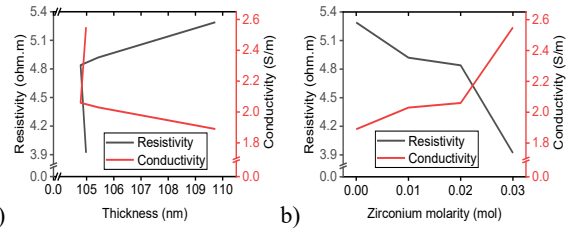

Figure 4: Plot of resistivity and conductivity Vs thickness and zirconium molarity

3.3 *Optical Study Of CrS and CrS/Zr Thin Film Synthesized At Different Dopant Concentration For Photovoltaic Application*

Figure 5 illustrates the absorbance, transmittance, reflectance, and bandgap energy of CrS and Zr-doped CrS material at different dopant concentrations. The absorbance decreases as the wavelength of light radiation increases from 300 to 1100 nm in Figure 5a. The absorbance decreases in the visible range from (400 – 600 nm) and the increase in the ultraviolet range from (700 – 1100 nm) of the spectra. The addition of zirconium dopant improved the synthesized material across both spectra regions. Zirconium dopant affects the absorbance of chromium sulfide material, especially at different molar concentrations. As the zirconium dopant concentration increases, so do the absorbance values. The concentration-dependent relationship between zirconium dopant and absorbance is evident [22]. The effect is less noticeable at lower concentrations (0.01 mol), but at higher concentrations (0.03 mol), there is a significant increase in absorbance. Zirconium ions in the material's structure modifies its electronic properties, causing shifts in light absorption behavior.

The transmittance increases as the wavelength of light radiation increases from 400 to 1100 nm. The transmittance increases in the visible range from (400 – 600 nm) and the increase continues to accumulate in the ultraviolet range from (300 – 400 nm) of the spectra in Figure 5b. The addition of zirconium dopant has been found to improve the transparency of chromium sulfide films with molar concentrations between 0.01 and 0.03 mol, enhancing the synthesized material across both spectra regions. Increasing the amount of zirconium dopant leads to better optical characteristics, including enhanced UV–VIS–NIR transmittance [22].

We conducted a study to find the ideal dopant level that improves transmittance by analyzing how zirconium doping affects chromium sulfide materials. The addition of zirconium enhances the photocatalytic activity of the materials. This implies that doping could have synergistic effects on chromium sulfide thin films, potentially resulting in improved optical and functional properties.

The reflectance decreases as the wavelength of light radiation increases from 300 to 1100 nm. The reflectance decreases in the visible range from (400 – 600 nm) and the increase in the ultraviolet range from (700 – 1100 nm) of the spectra in Figure 5c. Zirconium has altered the reflectance properties of chromium sulfide materials, deposited at different molar concentrations (0.01 to 0.03 mol) doping. The increase in zirconium dopant concentration causes a shift to lower wavelengths in the transmittance edge, resulting in a rise in overall reflectance. The dopant concentration in doped chromium sulfide and other chalcogenide materials can vary from 0.01 to 0.03 mol.

The experimental determination of the optimal dopant concentration is necessary for the desired reflectance and other properties. Tuned reflectance properties in zirconium-doped chromium sulfide materials have potential applications

in optoelectronics, energy storage, and catalysis. Being able to manipulate material properties through doping concentration is highly advantageous in material engineering and design. Doping with zirconium might modify the properties of materials, improving their characteristics for different uses [22]. As the zirconium dopant concentration increases, the optical band gap energy of chromium sulphide material decreases in Figure 5d, causing a shift in the transmittance edge to a lower wavelength. Doping with zirconium affects the thermodynamic, electronic, and optical characteristics of materials. The energy bandgap for CrS and Zr-doped CrS ranges from 2.35 to 1.55 eV [23], [24], [33], [25]–[32].

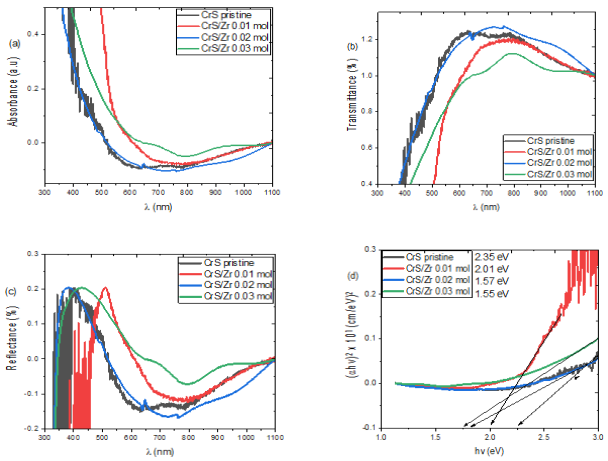

Figure 5: Plot of absorbance (a), transmittance (b), reflectance (c), and bandgap energy (d) Vs wavelength and photon energy

Figure 6 shows the refractive index, extinction coefficient, optical conductivity, and dielectric constants (both real and imaginary) of CrS and Zr-doped CrS material at different dopant concentrations in Figure 6a. The refractive index dictates how light bends as it passes through different substances, like water or glass. It's the ratio between the speed of light in a vacuum and the speed of light in a specific medium. The refractive index (n) is calculated by dividing the speed of light in vacuum by the speed of light in the medium. The refractive index becomes dimensionless due to the ratio of velocities.

The refractive index rises with an increase in photon energy. The addition of zirconium dopants influences the refractive index of chromium. Higher concentrations of zirconium doping result in an increase in the refractive index. The molar concentration of the zirconium dopant can influence the refractive index of the deposited material, ranging from 0.01 to 0.03 mol. Increasing the dopant's molar concentration leads to a higher refractive index.

The extinction coefficient explains how light weakens when it goes through a substance. The increase in zirconium (Zr) dopant concentration from 0.01 to 0.03 mol in chromium sulfide films resulted in a higher extinction coefficient for the material in Figure 6b. Zr doping has the potential to improve optical properties for optoelectronic applications. The extinction coefficient rises with increasing photon energy.

The optical conductivity of CrS and Zr-doped CrS rises with increasing photon energy. The optical conductivity of chromium sulfide (CrS) material can be influenced by the introduction of zirconium (Zr) as a dopant in Figure 6c. The tuning of optical properties in the CrS material is achieved by increasing the Zr doping concentration from 0.01 to 0.03 mol. Zr doping can alter the optical conductivity of the CrS material. The optical properties of the material can be adjusted by controlling the Zr doping level, as evidenced by the increasing optical conductivity values with higher Zr concentration.

The dielectric constant of zirconium-doped chromium sulfide changes based on factors such as dopant concentration and synthesis conditions in Figure 6d&e. The 0.03 mol Zr dopant material exhibited the highest imaginary dielectric constant. Doping chromium sulphide (CrS) materials with zirconium (Zr) affects their real and imaginary dielectric constant. By adjusting the Zr dopant concentration from 0.01 to 0.03 mol, the dielectric properties of CrS can be modified [22]. The dielectric constant of CrS materials, both real and imaginary, experienced notable variations with increasing Zr dopant concentration from 0.01 to 0.03 mol. The dielectric constant, both real and imaginary, increases slowly as photon energy rises.

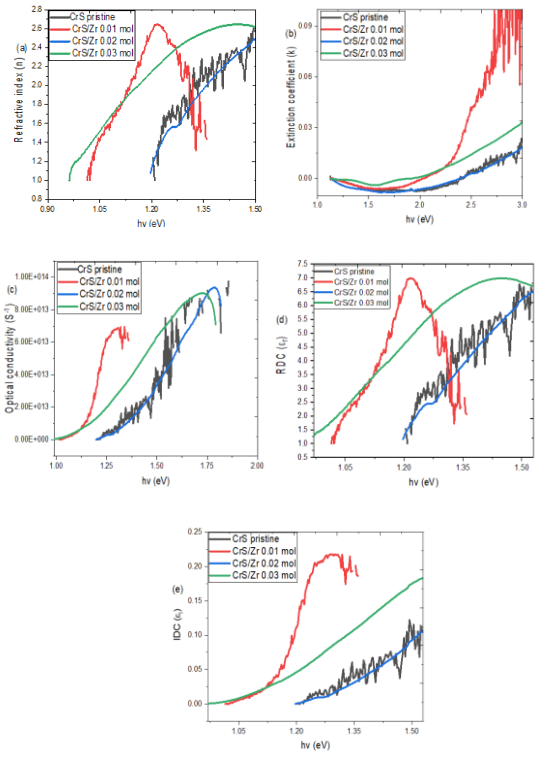

Figure 6: Plot of refractive index (a), extinction coefficient (b), optical conductivity (c), and real (d) and imaginary (e) dielectric constant Vs photon energy

4 Conclusions

The diffraction angle of CrS and Zr-doped CrS material at 2θ=25.256° and 27.009° confirmed the characteristic peak of CrS and Zr-doped CrS material. The XRD diffraction peaks at 2θ = 25.256°, 30.329°, 34.426°, 41.198°, 45.678°, 56.389° and 65.231° correspond respectively to the diffraction planes of 111, 112, 116, 200, 201, 211 and 300 of CrS materials. And the diffraction peaks at 2θ=27.009°, 34.321°, 38.471°, 52.345°, 55.177°, 62.397° and 66.548° correspond respectively to the diffraction planes of 111, 112, 116, 200, 201, 211 and 300 of Zr-doped CrS materials. The analysis reveals that the films contain nanoparticles of various sizes, from a few nanometers to tens of nanometers. At a dopant concentration of 0.01 M, the nanoparticles aggregate and have irregular shapes. When the concentration reaches 0.03 M, the irregular particles change into nano balls. The addition of zirconium dopant improved the synthesized material across the UV region. Zirconium dopant affects the absorbance of chromium sulfide material, especially at different molar concentrations. As the zirconium dopant concentration increases, so do the absorbance values. Zirconium has altered the reflectance properties of chromium sulfide materials, deposited at different molar concentrations (0.01 to 0.03 mol) doping. The increase in zirconium dopant concentration causes a shift to lower wavelengths in the transmittance edge, resulting in a rise in overall reflectance. The energy bandgap of CrS is 2.35 eV, but when Zr is doped into CrS, the energy bandgap ranges from 2.01 to 1.55 eV.

Acknowledgment

Our appreciation goes out to all the authors for their financial help, which was instrumental in the research's success.

Authors' Credit Statement

Laeticia U. Ugwu, Azubuike J. Ekpunobi and Imosobomeh L. Ikhioya: conceptualization, methodology, Data curation, **Azubuike J. Ekpunobi and Imosobomeh L. Ikhioya:** supervisor, data collection, first draft writing, reviewing, software, and editing**.** Investigation and visualization**.** All authors approved the submission.

Declaration of Competing Interest

The authors disclose no personal or financial conflicts that might have affected the research.

Reference

[1] Aftab, S., Iqbal, M. Z., Hussain, S., Hegazy, H. H., & Saeed, M. A. (2023). Transition metal dichalcogenides solar cells and integration with perovskites. *Nano Energy*, *108*. https://doi.org/10.1016/j.nanoen.2023.108249

[2] Afzal, S., Tehreem, S., Munir, T., Sarwar, S. G., & Ikhioya, I. L. (2023). *Impact of Transition Metal Doped Bismuth Oxide Nanocomposites on the Bandgap Energy for Photoanode Application*. *Journal of Nano and Materials Science Research*, *2*(1), 104–109. https://doi.org/10.20221/jnmsr.v2i1.14

[3] Agbrara, A. I., Ojegu, E. O., Osiele, M. O., & Ikhioya, I. L. (2023). Electrochemically Synthesize SrSe/ZrSe Heterostructure Material for Photovoltaic Application. *Advanced Journal of Chemistry, Section A*, *6*(4), 401–411. https://doi.org/10.48309/AJCA.2023.407032.1385

[4] Agobi, A. U., Ekpunobi, A. J., Ikeuba, A. I., Ikhioya, I. L., Chiaghanam, N. O., & Udofia, K. I. (2022). Hybrid polypyrrole/copper/graphene oxide nanocomposite films synthesized via potentiostatic deposition with enhanced photovoltaic properties. *Journal of the Indian Chemical Society*, *99*(7), 100549. https://doi.org/10.1016/j.jics.2022.100549

[5] Agobi, A. U., Ikeuba, A. I., Ekpunobi, A. J., Ikhioya, I. L., Udofia, K. I., Ntibi, J. E. E., Ozoemena, C. N., & Abua, M. A. (2023). Optical and structural properties of graphene oxide-incorporated polyvinylpyrrolidone/copper ternary nanocomposites (PVP/Cu/GO) films. *Revista Mexicana de Fisica*, *69*(3), 1–9. https://doi.org/10.31349/RevMexFis.69.031001

[6] Ahmad, I., Razzaq, J., Ammara, A., Kaleem, F., Qamar, M., Ilahi, S., & Ikhioya, I. (2024). Impact of Annealing Temperature on Hydrothermally Synthesized Copper Antimony Oxide (Cu2Sb2O) from Amorphous Phase to Monoclinic Structure. *Advanced Journal of Chemistry, Section A*, *7*(2), 110-121. doi: 10.48309/ajca.2024.419363.1429

[7] Akpu, N. I., Asiegbu, A. D., Nnanna, L. A., Ikhioya, I. L., & Mgbeojedo, T. I. (2022a). Influence of Substrate Temperature on the Photovoltaic/Optoelectronic properties of Spray-Synthesized Yttrium Copper Selenide (YCS) Thin Films. *Arabian Journal for Science and Engineering*, *47*(6), 7639–7646. https://doi.org/10.1007/s13369-021-06455-0

[8] Akpu, N. I., Asiegbu, A. D., Nnanna, L. A., Ikhioya, I. L., & Mgbeojedo, T. I. (2022b). Synthesis and characterization of novel yttrium-incorporated copper selenide (CuSe:Y) thin materials for solar energy applications. *Journal of Materials Science: Materials in Electronics*, *33*(3), 1154–1161. https://doi.org/10.1007/s10854-021-07397-x

[9] Akpu, N. I., Sylvanus, C. A., & Nwaokorongwu, E. C. (2023). *Modulation of the physical properties of spray-deposited cobalt selenide nanofilm via yttrium doping for photovoltaic purposes . J. Mater. Environ. Sci., 2023, Volume 14*, Issue 11, Page 1230-1244.

[10] Akpu, N., Okpechi, U., Elizabeth, N., Imosobomeh, I., Julian, O., Nnanna, L., & Agbodike, I. (2023). Impact

of temperature difference on the features of spray deposited yttrium doped cobalt selenide (YCoSe) thin films for photovoltaic application. *African Scientific Reports*, *2*, 143. https://doi.org/10.46481/asr.2023.2.3.143

[11] Ali, A., Afzal, S., Khaleeq, T., Shah, H., Usman, M., & Imosobomeh, L. (2023). *Synthesis and Characterization of Chitosan-Silver Nanocomposite Using Chemical Reduction Method and their Antibacterial Properties*. *Journal of Nano and Materials Science Research*, *2*(1), 117–122. https://doi.org/10.20221/jnmsr.v2i1.17

[12] Ali, F., & Yahaya, A. (2023). *Original Article: Improved Morphological, Structural, and Optical Features of Er*. *Journal of Applied Organometallic Chemistry*, *3*(4), 308-320. doi: 10.48309/jaoc.2023.421597.1127

[13] Nsude, H. E., Obodo, R. M., Nsude, K. U., Ikhioya, L. I., Asogwa, P. U., Osuji, R. U., Maaza, M., & Ezema, F. I. (n.d.). *Binder-free fabricated CuFeS 2 electrodes for supercapacitor applications Binder-free fabricated CuFeS 2 electrodes for supercapacitor applications*. *Mater. Res. Express* **9** 025501 doi.org/10.1088/2053-1591/ac4f13

[14] Chukwuemeka, E. J., Osita, N. A., Odira, A. O., Uchechukwu, U. C., Mimi, J. D., & Ikhioya, I. L. (2024). Performance and Stability Evaluation of Low-Cost Inorganic Methyl Ammonium Lead Iodide (CH3NH3PbI3) Perovskite Solar Cells Enhanced with Natural Dyes from Cashew and Mango Leaves. *Advanced Journal of Chemistry, Section A*, *7*(1), 27–40. https://doi.org/10.48309/ajca.2024.406961.1384

[15] Damisa, J., Emegha, J. O., & Ikhioya, I. L. (2021). Deposition Time induced Structural and Optical Properties of Lead Tin Sulphide Thin Films. *Journal of the Nigerian Society of Physical Sciences*, *3*(4), 455–458. https://doi.org/10.46481/jnsps.2021.157

[16] Danladi, E., Muhammad Y. Onimisi, Reuben M. Laah, & Imosobomeh L. Ikhioya. (2022). High Performance Dye Sensitized Solar Cells by Plasmonic Enhancement of Silver Nanoparticles in ZnO Photoelectrode with Betanin Pigment. *African Scientific Reports*, *1*(April), 1–15. https://doi.org/10.46481/asr.2022.1.1.3

[17] Emmanuel, O. C., Donald, O. N., & L. Ikhioya, I. (2022). Effect of Doping and Co-sensitization on the Photovoltaic Properties of Natural Dye-sensitized Solar Cells. *International Journal of Applied Physics*, *9*(3), 44–54. https://doi.org/10.14445/23500301/ijap-v9i3p105

[18] Hussain, A., Ali, F., & Hammad, H. (2024). Enhanced specific capacitance , structural , optical , and morphological study of carbon ions incorporated into the lattice of ZrCuO 2 nanoparticle synthesized by hydrothermal method. *Hybrid Advances*, *5*(January), 100170. https://doi.org/10.1016/j.hybadv.2024.100170

[19] Akpu, N., A.D, A., L.A, N., & L. Ikhioya, I. (2021). Investigation On The Influence of Varying Substrate Temperature On The Physical Features of Yttrium Doped Cadmium Selenide Thin Films Materials. *International Journal of Applied Physics*, *8*(2), 37–46. https://doi.org/10.14445/23500301/ijap-v8i2p106

[20] Idisi, D. O., & Mwakikunga, B. (2023). Two-dimensional layered metal dichalcogenides-based heterostructures for solar cells applications: A review. *Solar Energy*, *263*. https://doi.org/10.1016/j.solener.2023.111981

[21] Hussain, A., Habib, S., Ullah, I., Sahreen, F., Ahmad, I., & Ikhioya, I. (2024). Enhanced Structural, Morphological and Optical Features of Tix MnNiO (X= 1, 2, and 3 mL) Synthesized Using Hydrothermal Approach. *Eurasian Journal of Science and Technology*, *4*(3), 195-207. doi: 10.48309/ejst.2024.428429.1117

[21] Ikhioya, I. L., Aisida, S. O., Ahmad, I., & Ezema, F. I. (2023). The effect of molybdenum dopant on rare earth metal chalcogenide material. *Chemical Physics Impact*, *7*. https://doi.org/10.1016/j.chphi.2023.100269

[22] Josephine, E. N., Ikponmwosa, O. S., Alomayri, T., & Ikhioya, I. (2023). Enhanced physical properties of SnS/SnO semiconductor material. *Asian Journal of Nanoscience and Materials*, (), 199-212. doi: 10.26655/AJNANOMAT.2023.3.3

[23] Obitte, B. C. N., Ikhioya, I. L., Whyte, G. M., Chime, U. K., Ezekoye, B. A., Ekwealor, A. B. C., Maaza, M., & Ezema, F. I. (2022). The effects of doping and temperature on properties of electrochemically deposited Er3+ doped ZnSe thin films. *Optical Materials*, *124*(December 2021), 111979. https://doi.org/10.1016/j.optmat.2022.111979

[24] Ojegu, E. O., Odia, O. B., Osiele, M. O., Godfrey, A. E., & Ikhioya, I. L. (2023). *Effect of precursor temperature on electrochemically deposited zirconium doped chromium telluride using a standard three-electrode system*. *J. Mater. Environ. Sci., 2023,* Volume 14, Issue 11, Page 1148-1159

[25] Ojegu, E. O., Samuel, S. O., Osiele, M. O., Akpojotor, G. E., & Ikhioya, I. L. (2023). Optimisation of deposition voltage of zirconium-doped chromium telluride via typical three-electrode cell electrochemical deposition technique. *Materials Research Innovations*, *00*(00), 1–9. https://doi.org/10.1080/14328917.2023.2243063

[26] Ojegu, E. O., Samuel, S. O., Osiele, M. O., Akpojotor, G. E., & Ikhioya, I. L. (2024). Optimisation of deposition voltage of zirconium-doped chromium

telluride via typical three-electrode cell electrochemical deposition technique. *Materials Research Innovations*, *28*(3), 137–145. https://doi.org/10.1080/14328917.2023.2243063

[27] Rufus, I., Peter, A., Aisida, S. O., & Ikhioya, I. L. (2023). Results in Optics Influence of manganese molarity incorporation on manganese silver sulphide semiconductor material for photovoltaic applications. *Results in Optics*, *12*(February), 100464. https://doi.org/10.1016/j.rio.2023.100464

[28] Samuel, S. O., Frank, M. L. E., Ogherohwo, E. P., Ekpekpo, A., Zhimwang, J. T., & Ikhioya, I. L. (2023). Influence of Deposition Voltage on Strontium Sulphide Doped Silver for Optoelectronic Application. *East European Journal of Physics*, *2023*(1), 189–196. https://doi.org/10.26565/2312-4334-2023-1-25

[29] Samuel, S. O., Timothy, Z. J., Ojoba, C. K., & Ikhioya, L. (2023). *Original Research Article: Temperature's Impact on the Physical Properties of Rare Earth Element Doped SrS for Optoelectronic Use*.. *J. Eng. Ind. Res.* 2023, 4 (3):147-156. https://doi.org/10.48309/JEIRES.2023.3.2

[30] Sarwar, S. G., Ikhioya, I. L., Afzal, S., & Ahmad, I. (2023). Supercapitance performance evaluation of MXene / Graphene / NiO composite electrode via in situ precipitation technique. *Hybrid Advances*, *4*(September), 100105. https://doi.org/10.1016/j.hybadv.2023.100105

[31] Sumesh, C. K. (2019). Towards efficient photon management in nanostructured solar cells: Role of 2D layered transition metal dichalcogenide semiconductors. *Solar Energy Materials and Solar Cells*, *192*, 16–23. https://doi.org/10.1016/j.solmat.2018.12.016

[32] Udofia, K. I., Ikhioya, I. L., Okoli, D. N., & Ekpunobi, A. J. (2023). Impact of doping on the physical properties of PbSe chalcogenide material for photovoltaic application. *Asian Journal of Nanoscience and Materials*, *6*(2), 135–147. https://doi.org/10.26655/AJNANOMAT.2023.2.3